Superpenetration optical microscopy by iterative multiphoton adaptive compensation technique

Jianyong Tang[a], Ronald N. Germain[a], and Meng Cui[b,1]

[a]Laboratory of Systems Biology, National Institute of Allergy and Infectious Diseases, National Institutes of Health, Bethesda, MD 20892; and [b]Howard Hughes Medical Institute, Janelia Farm Research Campus, 19700 Helix Drive, Ashburn, VA 20147

Edited by* Erich P. Ippen, Massachusetts Institute of Technology, Cambridge, MA, and approved April 18, 2012 (received for review December 5, 2011)

Biological tissues are rarely transparent, presenting major challenges for deep tissue optical microscopy. The achievable imaging depth is fundamentally limited by wavefront distortions caused by aberration and random scattering. Here, we report an iterative wavefront compensation technique that takes advantage of the nonlinearity of multiphoton signals to determine and compensate for these distortions and to focus light inside deep tissues. Different from conventional adaptive optics methods, this technique can rapidly measure highly complicated wavefront distortions encountered in deep tissue imaging and provide compensations for not only aberration but random scattering. The technique is tested with a variety of highly heterogeneous biological samples including mouse brain tissue, skull, and lymph nodes. We show that high quality three-dimensional imaging can be realized at depths beyond the reach of conventional multiphoton microscopy and adaptive optics methods, albeit over restricted distances for a given correction. Moreover, the required laser excitation power can be greatly reduced in deep tissues, deviating from the power requirement of ballistic light excitation and thus significantly reducing photo damage to the biological tissue.

immunology | neuron imaging | nonlinear imaging | lymphocyte imaging | nonlinear iterative feedback

Optical microscopy has revolutionized biomedical research in the past few decades (1–15). Recent advances in spatial resolution (1, 16), labeling techniques (2, 11), imaging speed (7, 10), and new contrast mechanisms (4, 15, 17) have greatly expanded the capabilities of optical microscopy; however, a major drawback of this technique is the limited imaging penetration depth because biological tissues are rarely transparent (3, 6, 18, 19). Little advance has been made in imaging depth since the invention of multiphoton microscopy (MPM) (3) about two decades ago. Despite the development of tomography (6) and hybrid imaging techniques (18), MPM remains the most powerful and widely adopted technique for high resolution molecular and functional imaging (12). MPM allows observation of cellular and subcellular dynamics and functions in deep live tissue within highly complex and heterogeneous environments, providing critical in situ and in vivo information that is difficult to obtain otherwise. Long wavelength excitation can improve the imaging depth (20) but this limits the range of fluorophores that can be employed and still suffers from wavefront distortions (8, 17, 21). Extending the penetration depth has thus been a major challenge in studying extremely heterogeneous biological samples such as brain and lymphatic tissues.

Measuring and compensating for wavefront distortions lie within the realm of optical phase conjugation (OPC) (22) and adaptive optics (AO) (8, 17, 23, 24). The challenging task is to combine effectively well-established wavefront compensation techniques with deep tissue microscopy. OPC requires coherent wave mixing or interferometry. For fluorescence microscopy, the signal is incoherent, preventing the application of OPC. AO with wavefront sensors works with incoherent signals; however, the signal and the excitation differ in wavelength in MPM such that their wavefronts could be uncorrelated in thick tissues. A more practical solution is to modulate the excitation wavefront to maximize the emission power. Such a scheme was originally developed in the 1970s to focus a laser beam through air turbulence onto a remote target (25). Similar methods have also been explored to focus light through highly turbid media onto a point target or guide star (26–29). Despite progress in operation speed (26) and efficiency (27), none of the reported methods (26–31) have been applied to deep tissue microscopy in any practical way. The Achilles' heel of these methods is that a point target (size smaller than or comparable to the diffraction limit) or guide star is required to form a diffraction-limited focus inside highly turbid media, a condition rarely satisfied in practical imaging applications. Taking fluorescence microscopy as an example, the fluorophores could be distributed randomly inside samples and their distribution could be isolated or continuous over a volume much greater than the diffraction limit (7, 12).

Here, we introduce a wavefront modulation-based compensation technique that can form a diffraction-limited focus inside deep tissues without the requirement of point guide stars. We demonstrate application of this method to imaging of mouse brain slices and intact lymph nodes, with significant improvement of the depth of useful image generation accompanied by a reduction in input laser power required for such deep imaging. This approach paves the way for dynamic and functional intravital imaging at unprecedented depth.

Results

Different from previous work (26–31), the technique reported here has two different elements, iterative feedback and nonlinearity, and is named iterative multiphoton adaptive compensation technique (IMPACT). Fig. 1*A* shows the design of the superpenetration optical microscope that combines MPM with IMPACT. A tunable femtosecond oscillator is employed as the light source, whose power is regulated by an electro-optic (EO) modulator. The material dispersion of the setup is compensated by a prism pair compressor. Multiple relay lens pairs are used to image the x scan mirror to the y scan mirror then to a segmented deformable mirror (Kilo-DM, Boston Micromachines) and eventually to the rear pupil plane of a water immersion objective lens. The signal light is collected by the same lens and directed by a dichroic beam splitter onto a photomultiplier tube detector. The x and y galvo mirrors are used to create a raster-scanned image as in conventional MPM. The key element of the system is the high speed, segmented deformable mirror based on microelectromechanical systems (MEMS) technology, providing 32×32

Author contributions: M.C. designed the optical imaging system and carried out brain slice imaging; J.T. and R.N.G. designed the mouse lymph node study; J.T. and M.C. carried out lymph node imaging; M.C. analyzed the data; and J.T., R.N.G., and M.C. wrote the paper.

The authors declare no conflict of interest.

*This Direct Submission article had a prearranged editor.

Freely available online through the PNAS open access option.

[1]To whom correspondence should be addressed. E-mail: cuim@janelia.hhmi.org.

This article contains supporting information online at www.pnas.org/lookup/suppl/doi:10.1073/pnas.1119590109/-/DCSupplemental.

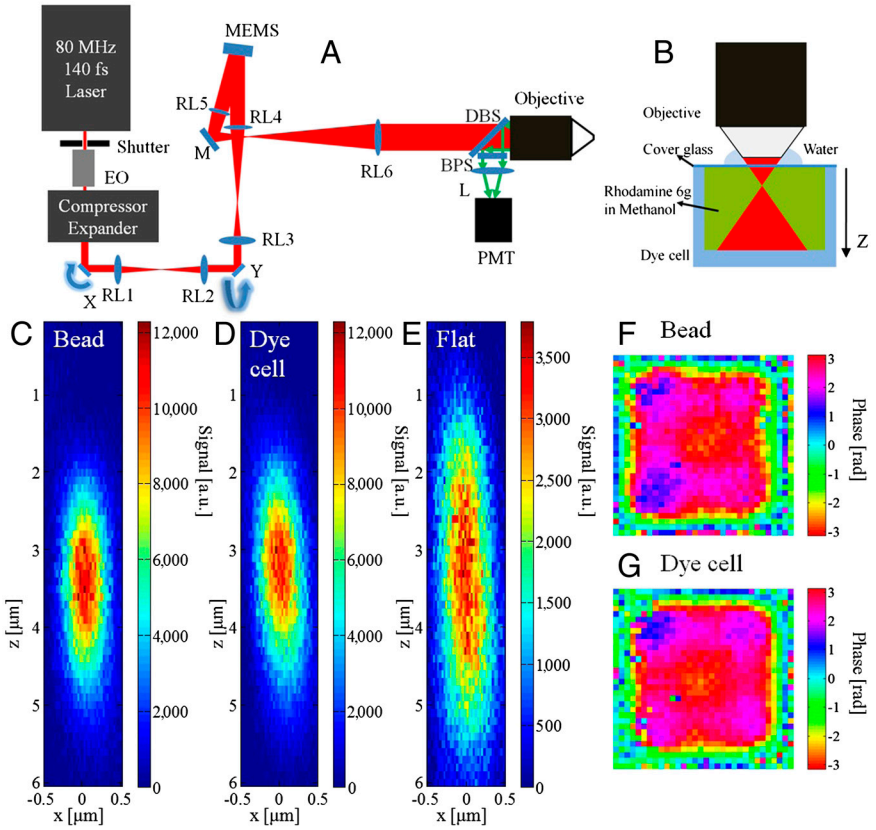

Fig. 1. Testing IMPACT's performance with large volume targets. (*A*) Setup of the superpenetration microscope. EO, electro-optic modulator; compressor, prism pair pulse compressor; expander, laser beam expander; RL1-6, relay lenses; DBS, long-pass dichroic beam splitter; BPS, band-pass filter; L:lens; Objective: NA 1.0 20x water immersion objective. (*B*) Setup for testing IMPACT with large volume targets. (*C*) PSF with the compensation profile determined with beads. (*D*) PSF with the compensation profile determined with dye cell. (*E*) PSF with a flat phase profile (no compensation). (*F*) Compensation profile determined with beads. (*G*) Compensation profile determined with dye cell.

segmented pixels with 20-μs response time and 1.5-μm stroke. The details of the system are described in the *Methods* section.

To test IMPACT's performance with large uniform targets, we used a glass cell filled with fluorescence dye as the sample (Fig. 1*B*). The two-photon fluorescence (TPF) signal was epidetected for wavefront compensation measurements. The IMPACT system needs to compensate for the aberration in the setup (system aberration) (Fig. S1*A*), and the aberration caused by the cover glass (Fig. S1 *B* and *C*). For comparison, we attached 0.1-μm diameter fluorescence beads under a cover glass (same type as in Fig. 1*B*) and used the beads as the target for IMPACT. After the wavefront was determined with the beads and the dye cell, we used the determined wavefront to perform three-dimensional (3D) TPF imaging of a single 0.1-μm bead to measure the point spread function (PSF). Fig. 1 *C*–*E* are the measured cross-sections of the PSF with the phase profiles measured with the bead (Fig. 1*F*), the dye cell (Fig. 1*G*), and a flat phase (no compensation) displayed on the MEMS mirror, respectively. The

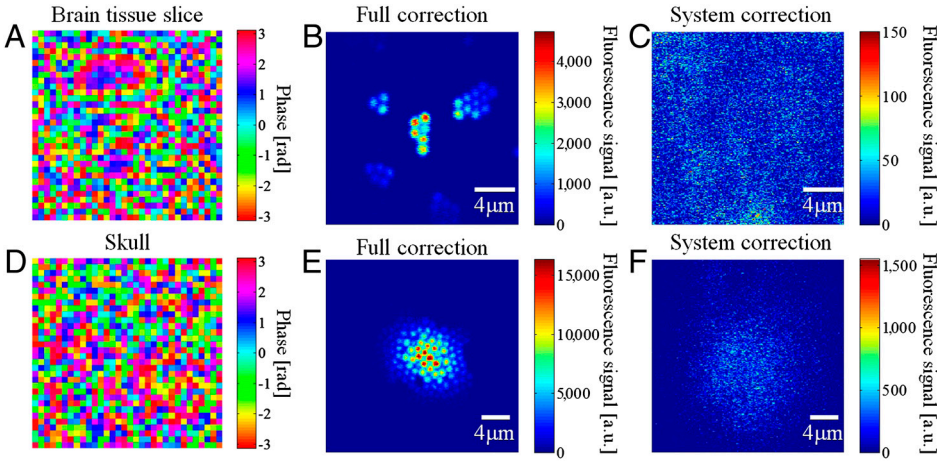

Fig. 2. Imaging through highly scattering sample. (*A*) Compensation profile determined through brain tissue. (*B*) TPF imaging through brain tissue with full correction. (*C*) TPF imaging through brain tissue with system correction. (*D*) Compensation profile determined through mouse skull. (*E*) TPF imaging through mouse skull with full correction. (*F*) TPF imaging through mouse skull with system correction.

comparison of the PSF and the determined phase profiles suggest that IMPACT can utilize large volume, uniform targets to form a focus.

To test the superpenetration microscope's performance with turbid biological samples, we placed a 400-μm thick slice of highly scattering mouse brain tissue and a piece of 150-μm thick mouse skull separately on top of a cover glass with 1-μm diameter fluorescence beads attached to the bottom. The goal was to see if IMPACT could compensate for the system aberration and the sample-induced wavefront distortion and form clear images of the beads underneath. Fig. 2*A* shows the compensation profile measured through the brain tissue. Fig. 2*B* shows the TPF images of the beads with full correction (system correction+ sample correction). For comparison, when only the system compensation profile was used, the TPF signal was reduced by approximately two orders of magnitude, and the image appeared as a random speckle (Fig. 2*C*). Because the wavefront distortions vary at different locations, the determined wavefront compensation is valid over a certain area near the measurement location. Therefore, in Fig. 2*B*, the image intensity decreases in regions away from the image center, where the wavefront measurement was performed. The corresponding data acquired through the mouse skull are shown in Fig. 2 *D–F*). TPF imaging of cortex in living mice often requires craniotomy or thinning the skull down to 25 μm (32). The TPF image in Fig. 2*E* suggests that IMPACT may potentially be used for TPF imaging through the intact skull. The signal strength comparison between Fig. 2 *B* and *C* suggests that the superpenetration microscope delivers more power to the focus than conventional MPM.

To investigate how the superpenetration microscope deviates from the ballistic power decay of conventional MPM, we used a fixed mouse brain with layer 5 neurons expressing GFP as the sample to compare the signal with full correction and with system correction. Fig. 3*A* shows the maximum intensity projection of the TPF image stacks acquired with conventional MPM. The scattering path length of the sample at the excitation wavelength 920 nm is estimated to be 129 ± 17 μm. The signal intensity at the dendrite is used as a measure of the focus power. The measured compensation profiles at 200-, 300-, and 400-μm depths are shown in Fig. 3 *B–D*, respectively. The TPF images acquired with full correction (Fig. 3 *E–G*) and system correction (Fig. 3 *H–J*) at these depths are also shown. The side views (maximum intensity projection) are shown in Fig. S2. At increased depth, the compensation profile becomes more complex and the images acquired with full correction show greater improvement in signal strength and image quality compared to the images acquired with only system correction. The intensity of the images as a function of imaging depth is shown in Fig. 3*K*. With only system correction, the signal follows a simple exponential decay since only the ballistic light component is used for TPF excitation. With full correction, the sample aberration is compensated for and the random scattering is suppressed such that more optical power

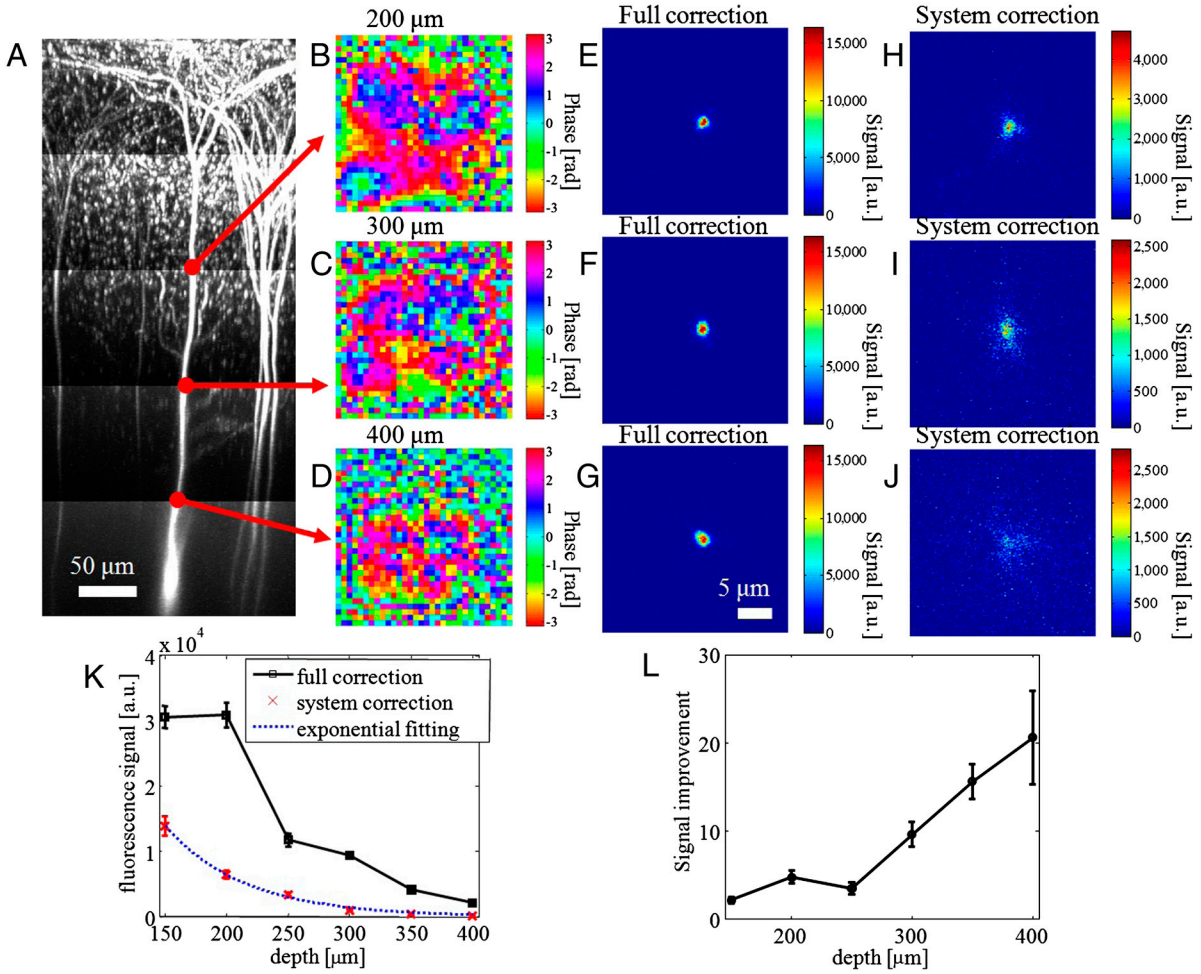

Fig. 3. Comparing signal decay curves. (*A*) Maximum intensity projection of GFP expressing layer 5 neurons acquired with conventional MPM. (*B–D*) Compensation profiles determined at 200-, 300-, and 400-μm depth, respectively. (*E–G*) TPF images of a dendrite with full correction at corresponding depths. (*H–J*) TPF images of a dendrite with system correction. (*K*) Image intensity as a function of depth with full correction and system correction. (*L*) The ratio of the two curves in *K*.

is delivered to the focus. Fig. 3*L* shows the ratio of the two curves in Fig. 3*K*. At 400-μm depth, IMPACT improves the image intensity by a factor of ~20.

To explore potential biomedical applications, we employed the superpenetration microscope to image GFP labeled T cells inside fixed lymph nodes. TPF image stacks were acquired from 0- to 800-μm depth. The scattering path length is estimated to be 124 ± 22 μm at the excitation wavelength 920 nm. The compensation profile measured at 800-μm depth is shown in Fig. 4*A*. Fig. 4*B* shows the volume view (view perpendicular to *z* axis) generated by ImageJ from an image stack (Movie S1) acquired with full correction and 60-mW excitation power at 800-μm depth. With only system correction, 300-mW excitation power is required to generate comparable signal strength; however, the image is blurry and has a large background due to out of focus excitation as shown in Fig. 4*C* (Movie S2). The reason for the segregation of GFP in T cells is under investigation and beyond the scope of this article.

For in vivo applications, samples are typically nonstationary, a significant challenge for accurate wavefront measurement. To study whether IMPACT can work on live animals and how long the measured wavefront remains valid, we performed in vivo imaging of mouse lymph nodes. For this study, we used the center 492 pixels of the MEMS mirror. The active pixels were arranged in an octagon shape that better matches the circular pupil of the objective lens. We injected 1-μm diameter fluorescence beads (Molecular Probes 505/515) into the footpad of the mouse. It took a few days for these beads to migrate deep into the lymph nodes carried by dendritic cells. Even at 80-μm depth, the sample-induced wavefront distortion is not negligible (Fig. S3). At the depth of 460 μm, IMPACT improves the signal intensity by more than one order of magnitude (Fig. 5*A* with full correction and Fig. 5*B*with system correction). The measured wavefront is shown in Fig. 5*C*. To study how long the measured wavefront remains valid, we switched between full correction and system correction every second during imaging. The consequent signal variation is shown in Fig. 5*D*. Over a measurement time of ~10 min, the signal improvement with a single IMPACT measurement remain above one order of magnitude.

Discussion

Comparison with Other Adaptive Optics Methods. Compared with other AO methods, IMPACT has four major advantages. First, conventional AO methods only compensate for low spatial frequency aberration. In contrast, IMPACT can measure and compensate for aberration and high spatial frequency wavefront distortion due to random scattering (Figs. 2 *A* and *B* and 4*A*). As a result, IMPACT not only improves image quality but also increases focusing efficiency. Randomly scattered light, regarded as a loss in MPM, can be coherently delivered to the focus by IMPACT, therefore, greatly reducing laser excitation power required for useful image generation. Second, conventional AO methods can only provide a very moderate (approximately two- to threefold) signal improvement in biological samples. We found IMPACT could improve signal strength by one to two orders of magnitude in highly scattering tissue. Third, conventional AO methods typically acquire wavefront information through multiple MPM images. Before the start of AO, a MPM image of reasonable quality needs to be generated for these methods to work. In highly scattering tissues, such a condition cannot be met (Fig. 2 *C* and *F*). In such cases, conventional AO methods will fail. IMPACT determines wavefront information though signal intensity variation, and it is shown to work in these highly scattering conditions. This scheme also minimizes photobleaching and photodamage in the majority of the imaging area. Fourth, IMPACT operates at higher speed. In current implementation, IMPACT can determine the phase profile of 1,024 independent spatial modes in a few seconds, ~10 times faster than image-based AO methods. The operation speed of IMPACT can potentially be further improved by a factor of ~10 with real-time software control of the MEMS mirror.

Benefits for Biological Studies. Most biological tissues have highly heterogeneous spatial structures with different regions having distinct functional activities and dynamics behavior. So, the ability to image deeper into tissues is likely to lead to discovery in many functional zones that were previously inaccessible. Our results demonstrate extended MPM penetration depth in brain and lymphoid tissues with high resolution as shown in the images of fine neuron dendrites (Fig. 3) as well as the small fluorescent clusters in T cells (Fig. 4). Moreover, the more efficient use of the laser light by IMPACT will significantly reduce the photobleaching and photodamage in the tissues that would minimize the artifacts in imaging due to strong light-matter interactions. Because IMPACT allows a larger portion of excitation laser energy to be distributed to the focal point, the imaging background is also suppressed so the improvement of image contrast is even better than the signal intensity improvement.

Large Field of View Imaging. One limitation of IMPACT is that the great improvement of signal strength is only valid for a limited volume. To quantify the dimensions of the improvement volume, we use the axially extended dendrite in Fig. 3 and the transversely extended beads in Fig. 2 to show the improvement range in the axial and transverse direction, respectively. The results are summarized in Fig. S4. The axial full width half maximum (FWHM) of the improvement is ~10 μm, though the image signal with full correction is much stronger than with system correction over a range of 20 μm or more. The transverse FWHM is less than 10 μm whereas the signal with full correction remains stronger over a ~10 μm area.

For applications requiring a large volume of view, we need to run IMPACT at different locations and combine the multiple small volumes into a large volume. Directly combining the images may suffer from a small amount of displacement error. In the current implementation, we use a mouse to click on the image to specify manually the parking spot of the Galvo scanner before IMPACT measurements. IMPACT will automatically focus light

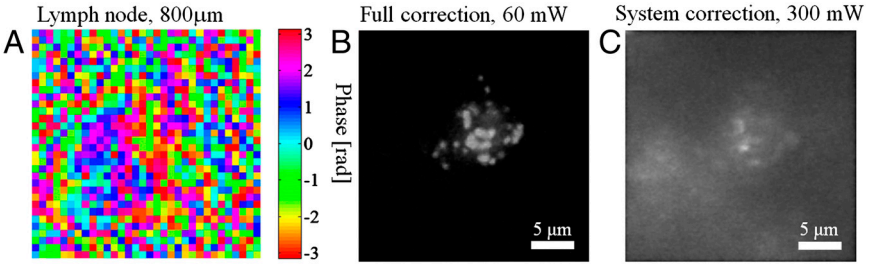

Fig. 4. Imaging GFP labeled T cells inside lymph nodes at 800-μm depth. (*A*) Compensation profile determined inside lymph node at 800-μm depth. (*B*) Volume view of the image stacks acquired at 800-μm depth with full correction and 60-mW excitation power. (*C*) Volume view of the image stacks acquired at 800-μm depth with system correction and 300-mW excitation power.

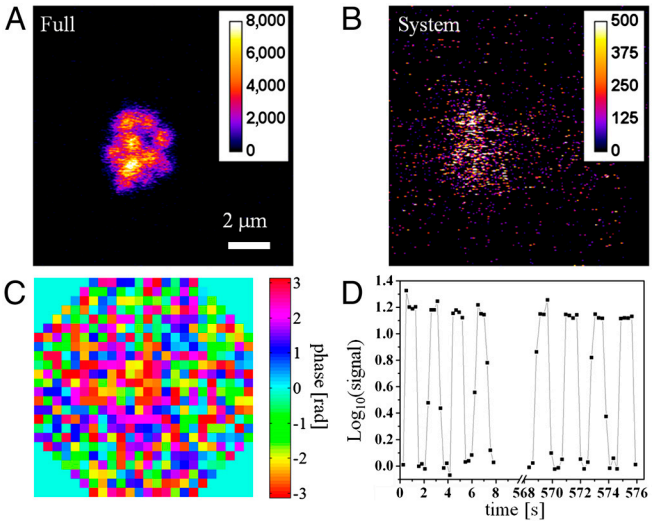

Fig. 5. In vivo imaging of mouse lymph node. One micron diameter fluorescence beads at 460-μm depth inside lymph node imaged with full correction (*A*) and system correction (*B*). (*C*) The full correction wavefront. (*D*) The image intensity variation due to periodic switching between full correction and system correction.

onto a local maximum (the brightest spot). If the initial parking spot we manually selected is not the brightest spot in the neighborhood, the wavefront measured by IMPACT will contain a certain amount of tilt. Such an effect is shown in Fig. S5. To minimize such displacement errors, we need to ensure that neighboring IMPACT measurement locations are close enough such that there are overlapping effective areas that allows us to use conventional image stitching software to correct the displacement error and yield a large image. One demonstration of using IMPACT for large area imaging is shown in Fig. S6.

With 492 active pixels on the MEMS mirror, currently IMPACT requires ~2.4 s to complete three iterations. If there are 20 different area of interest, we need to use ~48 s for wavefront measurement. In the following time, we can quickly switch between these 20 wavefronts at 2.5 kHz to monitor these areas of interest over time. Based on the in vivo imaging results (Fig. 5), the measured wavefront remains valid after ~10 min, which suggests that there is no need to repeat wavefront measurement in this time period. Because the total wavefront measurement time accounts for less than 8% of the total imaging time, the speed reduction of the imaging process is not dramatic.

The accurate measurement of the local wavefront requires a sufficient feedback optical signal so it is preferable to have bright reference signal of different color in the tissue if the cells of interest are not bright enough. This can be achieved by injecting bright chromophores such as quantum dots into the blood vessels or using cell-borne fluorescent microspheres like the beads carried by dendritic cells shown in the in vivo experiment. Such protocols are regularly used in intravital imaging. Moreover, the second harmonic generation (SHG) signal that is available in many types of tissues can also be used as feedback signal.

Conclusion

We report a superpenetration optical microscope based on IMPACT that takes advantage of the nonlinearity of MPM signals and iterations to form a focus inside turbid samples rapidly without the requirement of point guide stars. The microscope was employed to image through highly scattering mouse brain tissue, a mouse skull, inside a fixed mouse brain, and inside mouse lymph nodes. Compared to conventional MPM, the superpenetration microscope based on IMPACT can acquire clear images in deep tissues with a greatly reduced requirement for excitation power. Additionally, the background signals due to out of focus excitation, a limitation for deep tissue MPM (21), can be greatly reduced because IMPACT suppresses random scattering and delivers power more efficiently to the focus. The limitation is that the imaging field of view achieved with one wavefront compensation is limited. To see a large area, multiple wavefront compensations need to be performed at different locations and the acquired images need to be stitched (Fig. S6). T cell imaging in lymph nodes was explored, and the field of view with one wavefront compensation is sufficient to capture an entire T cell at 800-μm depth. In vivo imaging was performed on mouse lymph node, which shows that the wavefront acquired with a single IMPACT measurement remains valid after ~10 min. The combination of high quality imaging, low-excitation power, and low background makes the IMPACT based superpenetration optical microscope a promising tool for a broad range of biomedical applications. In particular, it paves the way for intravital functional and dynamic imaging at unprecedented depth beneficial for in vivo studies involving highly turbid samples including, but not limited to, neuroscience (33) and immunology (34, 35).

Methods

Operation of the Superpenetration Microscope. IMPACT takes five steps for wavefront compensation. In step one, the x and y scanning mirrors are stopped such that the laser beam is parked at a location of interest. In step two, half of the MEMS phase elements (512 elements) are modulated simultaneously with each element at a unique frequency. The other 512 elements are kept stationary. The power of the generated nonlinear signal is recorded during the parallel phase modulation. In step three, at the end of the phase modulation, the recorded nonlinear signal is Fourier transformed and the phase values of the 512 elements are extracted from the corresponding modulation frequencies and sign reversed before being applied to the 512 modulated elements. In step four, the newly measured 512 elements are kept stationary while the other 512 elements go through step two and three. In step five, steps two through four are repeated twice, which concludes the wavefront compensation. At this point, a focus is formed inside turbid tissues, x and y mirrors start scanning, and the objective is translated in the *z* axis to acquire three-dimensional MPM image stacks around the wavefront compensation location.

Three iterations were used to determine the compensation wavefront for all the experiments reported here. In each iteration, the minimum number of modulations required for determining 1,024 phase values is 2,048 (Nyquist-Shannon sampling theorem). In experiments, 4,096 modulations were used (2,048 modulation per 512 pixels). The update rate of the MEMS mirror in the experiment was 2.5 kHz. The modulation frequencies for the 512 modulated pixels were uniformly distributed between 0.625 and 1.25 kHz. The total modulation time for three iterations is ~5 s. The operation speed of the MEMS mirror was limited by the control software. Potentially, the update rate can reach 30 kHz reducing the total modulation time to ~0.4 s. The laser power was regulated (gradually lowered) during the IMPACT measurements to maintain a consistent DC value of the generated nonlinear signal.

The dwell time for all the TPF images reported here was 5 μs/pixel except for Fig. 3*A*, Fig. 5, and Fig. S3 in which 2.5 μs/pixel was used. The laser power at the sample was 3.6 mW in Fig. 1 *C*–*E*; 60 mW in Fig. 2 *B* and *C*; 12 mW in Fig. 2 *E* and *F*; 3.9 mW in Fig. 3 *E* and *H*; 7.2 mW in Fig. 3 *F* and *I*; 15 mW in Fig. 3 *G* and *J*; 14 mW in Fig. 5; 1.75 mW in Fig. S3; 77 mW in Fig. S5*A*; 97 mW in Fig. S5*B*; and 140 mW in Fig. S6. Fig. 3*A* was from five image stacks 100-μm depth in each stack. Starting from the top, the laser power used for the five image stacks is 24, 36, 54, 96, and 180 mW. The power used during IMPACT wavefront measurements was typical 2–3 times the TPF imaging power.

To determine the system compensation profile, we immobilized 1-μm diameter fluorescence beads in agar, immersed the sample in water, and performed IMPACT measurements. The determined compensation profile is shown in Fig. S1*A*. The phase differences between the system compensation and Fig. 1 *F* and *G* are shown in Fig. S1 *B* and *C*), respectively, which shows the aberration caused by the cover glass.

Interpretation of IMPACT Operation. The wavefront compensation and focus formation can be explained as nonlinearity assisted iterative optical phase conjugation. During the parallel phase modulation in step two, the *E* field (E_i) controlled by each of the 512 modulated elements interferes with the reference *E* field (E_r) controlled by the 512 stationary phase elements. For a single point source (guide star), the signal is strongest when E_i and E_r are in phase at the guide star location. Through step two and three, the cor-

rect phase value that makes E_i and E_r in phase can be determined, and the newly measured 512 phase elements are ready to perform a phase conjugation and focus the laser beam onto the guide star. If multiple guide stars are present, the phase conjugation beam will focus onto multiple locations with stronger guide stars receiving stronger illumination. In step four, the phase conjugation beam serves as the reference field to determine the phase profile for the other 512 phase elements. Different from step two, the new reference field now preferentially illuminates stronger guide stars further increasing the signal contribution from these stronger guide stars. If the two groups of phase elements take turns serving as the reference field and are measured iteratively as described in step five eventually a focus is formed onto the strongest guide star. For linear signals, such a scheme will fail to form a focus if the target is uniform and occupies a large volume, for example, a laser beam focused inside a glass cell filled with fluorescence dye (Fig. 1*B*); however if the signal generation involves higher order processes such as TPF or SHG, the nonlinearity can assist the formation of a single focus. Essentially, the entire process of phase modulation and compensation is to optimize the excitation wavefront to maximize the generated signals. If the beam is immersed in a large and uniform target as in Fig. 1*B*, the phase-only modulation cannot cause any variation of the total signal given that the signal is generated through a linear process; however, nonlinearity favors the formation of a focus because the overall signal is stronger if a single focus is formed inside the sample. Although how the 3D nonlinear iterative feedback system converges is difficult to analyze, experiments on a variety of samples show that three iterations are often sufficient to yield a high quality focus inside turbid tissues.

Mouse Lymph Node Preparation for in Vitro and in Vivo Imaging. ***Fixed sample.*** The T-bet reporter mouse harbors a BAC transgene in which the ZS-green version of GFP fluorescent protein is expressed under control of the T-bet promoter. The popliteal lymph nodes were harvested from the euthanized mouse and fixed in PLP buffer (1% paraformaldehyde, 2.12 g/L periodate, and 0.07 M L-lysine in 0.1 M phosphate buffer) overnight. The lymph nodes were then washed in PBS buffer and embedded in 4% agarose gel for imaging.

In vivo imaging. Fluorescent microspheres (Invitrogen, 1 μm in diameter) are resuspended in PBS and mixed with lipopolysaccharide (LPS) as adjuvant. The mouse is anesthetized using isoflurane inhalation and intracutaneous injections of beads (10^7 to 10^8) and LPS (25 μg) is then performed. After 2–3 d, the mouse is anesthetized by continuous inhalation of isoflurane and immobilized on a homemade stage. The popliteal lymph node is carefully exposed by surgery and the mouse moved into the microscope for imaging using continuous anesthesia. A soft heating pad is used to keep the mouse and stage warm during imaging.

All procedures involving mice were approved by the Animal Care and Use Committees of National Institute of Allergy and Infectious Diseases, National Institutes of Health, and of Howard Hughes Medical Institute.

ACKNOWLEDGMENTS. The authors thank Charles Shank, Na Ji, Eric Betzig, Mats Gustafsson, and Karel Svoboda for helpful discussions. We also thank Wolfgang Kastenmuller and Michael Gerner for help on live mouse imaging. Jeff Zhu (National Institutes of Health) kindly provided the T-bet:GFP mice. The research is supported by Howard Hughes Medical Institute and Intramural Research Program of the National Institute of Allergy and Infectious Diseases, National Institutes of Health.

1. Betzig E, et al. (2006) Imaging intracellular fluorescent proteins at nanometer resolution. *Science* 313:1642–1645.
2. Chalfie M, Tu Y, Euskirchen G, Ward WW, Prasher DC (1994) Green fluorescent protein as a marker for gene-expression. *Science* 263:802–805.
3. Denk W, Strickler JH, Webb WW (1990) 2-Photon laser scanning fluorescence microscopy. *Science* 248:73–76.
4. Freudiger CW, et al. (2008) Label-free biomedical imaging with high sensitivity by stimulated raman scattering microscopy. *Science* 322:1857–1861.
5. Helmchen F, Denk W (2005) Deep tissue two-photon microscopy. *Nat Methods* 2:932–940.
6. Huang D, et al. (1991) Optical Coherence Tomography. *Science* 254:1178–1181.
7. Huisken J, Swoger J, Del Bene F, Wittbrodt J, Stelzer EHK (2004) Optical sectioning deep inside live embryos by selective plane illumination microscopy. *Science* 305:1007–1009.
8. Ji N, Milkie DE, Betzig E (2010) Adaptive optics via pupil segmentation for high-resolution imaging in biological tissues. *Nat Methods* 7:141–U184.
9. Keller PJ, et al. (2010) Fast, high-contrast imaging of animal development with scanned light sheet-based structured-illumination microscopy. *Nat Methods* 7:637–642.
10. Planchon TA, et al. (2011) Rapid three-dimensional isotropic imaging of living cells using Bessel beam plane illumination. *Nat Methods* 8:417–U468.
11. Tsien RY (1998) The green fluorescent protein. *Annu Rev Biochem* 67:509–544.
12. Wilt BA, et al. (2009) Advances in light microscopy for neuroscience. *Annu Rev Neurosci* 32:435–506.
13. Xu C, Zipfel W, Shear JB, Williams RM, Webb WW (1996) Multiphoton fluorescence excitation: New spectral windows for biological nonlinear microscopy. *Proc Natl Acad Sci USA* 93:10763–10768.
14. Zipfel WR, Williams RM, Webb WW (2003) Nonlinear magic: Multiphoton microscopy in the biosciences. *Nat Biotechnol* 21:1369–1376.
15. Zumbusch A, Holtom GR, Xie XS (1999) Three-dimensional vibrational imaging by coherent anti-Stokes Raman scattering. *Phys Rev Lett* 82:4142–4145.
16. Bates M, Huang B, Dempsey GT, Zhuang XW (2007) Multicolor super-resolution imaging with photo-switchable fluorescent probes. *Science* 317:1749–1753.
17. Debarre D, et al. (2009) Image-based adaptive optics for two-photon microscopy. *Opt Lett* 34:2495–2497.
18. Wang LV (2009) Multiscale photoacoustic microscopy and computed tomography. *Nat Photonics* 3:503–509.
19. Yaqoob Z, Psaltis D, Feld MS, Yang C (2008) Optical phase conjugation for turbidity suppression in biological samples. *Nat Photonics* 2:110–115.
20. Kobat D, et al. (2009) Deep tissue multiphoton microscopy using longer wavelength excitation. *Opt Express* 17:13354–13364.
21. Theer P, Hasan MT, Denk W (2003) Two-photon imaging to a depth of 1000 mu m in living brains by use of a Ti : Al2O3 regenerative amplifier. *Opt Lett* 28:1022–1024.
22. Gower M, Proch D (1994) *Optical Phase Conjugation* (Springer-Verlag, New York).
23. Rueckel M, Mack-Bucher JA, Denk W (2006) Adaptive wavefront correction in two-photon microscopy using coherence-gated wavefront sensing. *Proc Natl Acad Sci USA* 103:17137–17142.
24. Tsai PS, et al. (2007) Spherical aberration correction in nonlinear microscopy and optical ablation using a transparent deformable membrane. *Appl Phys Lett* 91:191102.
25. Bridges WB, et al. (1974) Coherent optical adaptive techniques. *Appl Optics* 13:291–300.
26. Cui M (2011) A high speed wavefront determination method based on spatial frequency modulations for focusing light through random scattering media. *Opt Express* 19:2989–2995.
27. Cui M (2011) Parallel wavefront optimization method for focusing light through random scattering media. *Opt Lett* 36:870–872.
28. Katz O, Small E, Bromberg Y, Silberberg Y (2011) Focusing and compression of ultrashort pulses through scattering media. *Nat Photonics* 5:372–377.
29. Vellekoop IM, Mosk AP (2007) Focusing coherent light through opaque strongly scattering media. *Opt Lett* 32:2309–2311.
30. Hsieh CL, Pu Y, Grange R, Laporte G, Psaltis D (2010) Imaging through turbid layers by scanning the phase conjugated second harmonic radiation from a nanoparticle. *Opt Express* 18:20723–20731.
31. Vellekoop IM, Aegerter CM (2010) Scattered light fluorescence microscopy: imaging through turbid layers. *Opt Lett* 35:1245–1247.
32. Yang G, Pan F, Parkhurst CN, Grutzendler J, Gan WB (2010) Thinned-skull cranial window technique for long-term imaging of the cortex in live mice. *Nat Protoc* 5:201–208.
33. Svoboda K, Yasuda R (2006) Principles of two-photon excitation microscopy and its applications to neuroscience. *Neuron* 50:823–839.
34. Lizana A, et al. (2008) Time fluctuations of the phase modulation in a liquid crystal on silicon display: characterization and effects in diffractive optics. *Opt Express* 16:16711–16722.
35. Germain RN, Miller MJ, Dustin ML, Nussenzweig MC (2006) Dynamic imaging of the immune system: progress, pitfalls and promise. *Nat Rev Immunol* 6:497–507.